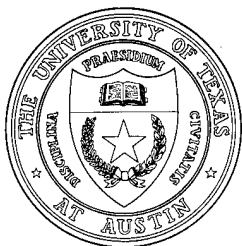ARL-TR-94-21

Copy No. _56_

# Bottom Backscatter from Trapped Bubbles - II
### Final Report under Contract N00039-91-C-0082
TD No. 01A2063, Bottom Backscatter from Trapped Bubbles - II

Frank A. Boyle
Nicholas P. Chotiros

## Applied Research Laboratories
### The University of Texas at Austin
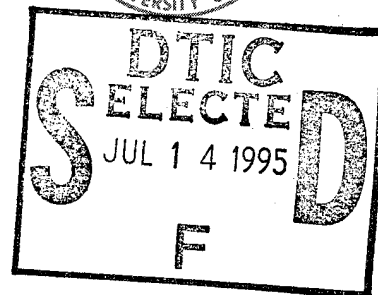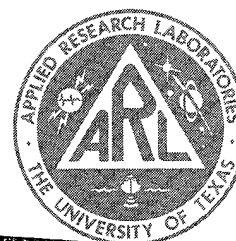P. O. Box 8029     Austin, TX 78713-8029

1 December 1994

Final Report

15 April 1993 - 15 April 1994

Approved for public release;
distribution is unlimited.

*Prepared for:*
**Naval Research Laboratory**
**Stennis Space Center, MS  39529-5004**

*Monitored by:*
**Space and Naval Warfare Systems Command**
**Department of the  Navy**
**Arlington, VA  22245-5200**

# UNCLASSIFIED

## REPORT DOCUMENTATION PAGE

Form Approved
OMB No. 0704-0188

| 1. AGENCY USE ONLY (Leave blank) | 2. REPORT DATE | 3. REPORT TYPE AND DATES COVERED |
|---|---|---|
| | 1 Dec 94 | final   15 Apr 93 - 15 Apr 94 |

**4. TITLE AND SUBTITLE**

Bottom Backscatter from Trapped Bubbles - II, Final Report under Contract N00039-91-C-0082, TD No. 01A2063, Bottom Backscatter from Trapped Bubbles - II

**5. FUNDING NUMBERS**

Contract N00039-91-C-0082
TD No. 01A2063

**6. AUTHOR(S)**

Boyle, Frank A.          Chotiros, Nicholas P.

**7. PERFORMING ORGANIZATION NAMES(S) AND ADDRESS(ES)**

Applied Research Laboratories
The University of Texas at Austin
P.O. Box 8029
Austin, TX  78713-8029

**8. PERFORMING ORGANIZATION REPORT NUMBER**

ARL-TR-94-21

**9. SPONSORING/MONITORING AGENCY NAME(S) AND ADDRESS(ES)**

Naval Research Laboratory
Stennis Space Center, MS 39529-5004

Space and Naval Warfare
Systems Command
Department of the Navy
Arlington, VA  22245-5200

**10. SPONSORING/MONITORING AGENCY REPORT NUMBER**

**11. SUPPLEMENTARY NOTES**

**12a. DISTRIBUTION/AVAILABILITY STATEMENT**

Approved for public release; distribution is unlimited.

**12b. DISTRIBUTION CODE**

**13. ABSTRACT (Maximum 200 words)**

A model for acoustic backscatter from trapped gas bubbles in sandy sediments was described in "Bottom Backscatter from Trapped Bubbles," Applied Research Laboratories Technical Report No. 93-15 (ARL-TR-93-15). In that model, trapped bubbles were assumed to scatter as if they were free bubbles in open water. In this report, the effects of bubble confinement in sediment pores on the resonance behavior of the bubble are accounted for. This is done by assigning the pore fluid an effective density that differs from its actual density, accounting for the fact that the fluid is partially confined within pores. The effective density is computed by way of the Biot theory. Two effective densities are specified, one for each of the two compressional waves that the Biot theory predicts. As a result, the medium has two scattering cross sections, which are both included in the resulting expression for scattering strength.

**14. SUBJECT TERMS**

| acoustic impedance | bubble | pore pressure | scattering cross section |
|---|---|---|---|
| backscatter | effective density | reciprocity | shallow grazing angle |
| Biot | gas | sandy sediments | |

**15. NUMBER OF PAGES**

29

**16. PRICE CODE**

| 17. SECURITY CLASSIFICATION OF REPORT | 18. SECURITY CLASSIFICATION OF THIS PAGE | 19. SECURITY CLASSIFICATION OF ABSTRACT | 20. LIMITATION OF ABSTRACT |
|---|---|---|---|
| UNCLASSIFIED | UNCLASSIFIED | UNCLASSIFIED | SAR |

NSN 7540-01-280-5500

## UNCLASSIFIED

This page intentionally left blank.

# TABLE OF CONTENTS

This page intentionally left blank.

# LIST OF FIGURES

This page intentionally left blank.

# PREFACE

This document is the final report on work that Applied Research Laboratories, The University of Texas at Austin (ARL:UT), was tasked to perform under Contract N00039-91-C-0082, TD No. 01A2063, Bottom Backscatter from Trapped Bubbles - II.

This page intentionally left blank.

# EXECUTIVE SUMMARY

In "Bottom Backscatter from Trapped Bubbles" by Boyle and Chotiros[2] a model for shallow grazing angle acoustic backscatter from sandy sediments was developed. It included a Biot model for acoustic propagation and a scattering mechanism from trapped bubbles in the sediment pores. One of the assumptions made was that the resonance frequencies and scattering cross sections of trapped bubbles are the same as those the bubbles would have if they were surrounded by open water. The possible effects of confinement within sediment pores were neglected. In this report, a revised expression for the sediment backscattering strength is developed that includes the effects of bubble confinement in pores.

The Biot slow and fast compressional waves are considered separately. Shear waves are neglected because they do not couple strongly into the pore fluid. There are separate acoustic impedances and scattering cross sections, specific for the fast and slow waves. The scattering problem is treated separately for each of the two wave types. The total scattering cross section includes components from both waves.

The model requires a number of input parameters. There are methods to measure or estimate all but two. They are (1) the sediment pore fluid gas fraction and (2) the bubble radius to pore radius ratio ($r_{bp}$). These are treated as free parameters.

Model predictions are compared with backscatter data from four sites. The model, by adjustment of its free parameters, can be made to fit the observations. This supports the hypothesis that trapped gas bubbles may be a significant source of acoustic backscatter in sediments.

Very small gas fractions of $10^{-5}$ to $10^{-6}$ are sufficient to fit observed levels of backscatter. There is no practical way to measure such small gas fractions at present, so an independent verification is not presently available.

The bubble size to pore size ratio required to fit grain size dependence of existing backscatter data is unreasonably large. This ratio also increases

steadily as the sediment grain size decreases. This behavior casts doubt on the accuracy of the current method of estimating trapped bubble sizes, specifically, that the bubble size distribution is proportional to the pore size distribution. A more accurate way of estimating bubble size distribution is needed.

The values of the input parameters that fit the model to existing backscatter measurements appear to be reasonable. The fact that the bubble to pore radius ratio is greater than unity suggests that other factors besides pore size influence the size of a trapped bubble. When a more accurate estimate of the bubble size distribution becomes available, it can be incorporated into the model. Until then, the current technique allows a semi-empirical estimate of bubble size distribution, which results in a reasonable fit of the model to observed backscatter data.

# 1. INTRODUCTION

The objective of this work is an improved model for high frequency acoustic backscatter from sandy sediments at shallow grazing angles. Initial development of the model was described by Boyle and Chotiros in 1992.[1] In this initial work, a comprehensive compilation of shallow grazing angle backscatter measurements was presented. Some of the data featured a broad maximum in the backscattering strength spectrum that was not explainable with current models. A new hypothetical mechanism for acoustic backscatter was proposed, involving resonance scattering from trapped gas bubbles. A preliminary backscatter model based on this scattering mechanism was then developed. In 1993, a more complete model[2] was developed that combined a Biot propagation model with a trapped bubble backscatter model. The model included a means of estimating the trapped bubble size distribution from the grain size distribution, based on the assumption that the bubble size distribution mirrors the pore size distribution.

One of the assumptions made in the 1993 model is that trapped bubbles respond acoustically as if they are free bubbles surrounded by water. In this report, the acoustic response of bubbles that are constrained within sediment pores is investigated. The presence of solid particles in the fluid surrounding the bubbles is accounted for. The result is a new model with no assumptions regarding the bubbles' confinement in the sediment.

This report is arranged as follows: in Sec. 2 a theoretical model is developed to describe the acoustic response of bubbles trapped in sediment. Section 3 contains comparisons between model predictions and experimental measurements. A discussion of the results follows in Sec. 4.

This page intentionally left blank.

## 2. TRAPPED BUBBLE BACKSCATTERING STRENGTH

The objective of the backscatter model is an expression for the backscattering strength of the sediment interface, due to scattering from bubbles in the volume below the interface. The acoustic response of the bubbles is influenced by the fact that the bubbles are confined in pores between sand grains.

Sediment particles influence the acoustic behavior of bubbles because they affect the effective density of the surrounding fluid medium. This effective density is the density of an equivalent unbounded fluid, in which bubbles would have the same acoustic response that they have in sandy sediment.

The influence of the effective density manifests itself in two ways. First, the backscattering cross section of each bubble is affected by the density of the surrounding fluid. Second, the relationship between incident and backscattered pressure, which is developed from the reciprocity principle,[3,4] is affected by the impedance difference across the sediment boundary. The two effects are discussed separately in Secs. 2.1 and 2.2 below. Section 2.3 is a discussion of how pore fluid effective densities and pressures are determined by way of the Biot theory. In Sec. 2.4 the pore pressure is used to obtain an expression for the sediment backscattering strength.

In the following analysis, complex quantities are printed in boldface. Real quantities are plain text.

## 2.1   BACKSCATTERING CROSS SECTION OF A CONSTRAINED BUBBLE

In this section, an expression is presented for the acoustic scattering cross section of a bubble in terms of the density of the surrounding fluid. An expression for the appropriate value for this density is later presented in Sec. 2.3.

The backscatter model described in Ref. 2 uses the expression for the scattering cross section of a single spherical bubble, given by Wildt[5]:

$$\sigma_r(r_b) = \frac{4\pi r_b^2}{\left[\left(\frac{f_r}{f}\right)^2 - 1\right]^2 + \delta^2} \quad , \tag{2.1}$$

where $\sigma_r$ is the scattering cross section, $r_b$ is the bubble radius, $f$ is the incident acoustic frequency, $f_r$ is the resonance frequency, and $\delta$ is the damping constant, given by

$$\delta = k r_b + \frac{d}{b}\left(\frac{f_r}{f}\right)^2 + \frac{4\mu}{\rho \omega_r r_b^2} \quad , \tag{2.2}$$

where $k$ is the acoustic wavenumber in the surrounding medium; $\mu$ is the shear viscosity of the fluid; $\rho$ is the density of the medium surrounding the bubbles; $\omega_r = 2\pi f_r$ is the angular resonance frequency; $d/b$ is given by

$$\frac{d}{b} = 3(\gamma-1)\frac{X(\sinh X + \sin X) - 2(\cosh X - \cos X)}{X^2(\cosh X - \cos X) + 3(\gamma-1)X(\sinh X - \sin X)} \quad , \tag{2.3}$$

where $\gamma$ is the ratio $C_p/C_v$ of specific heats for the gas inside the bubble; and $X$ is given by

$$X = r_b \sqrt{\frac{2\omega_r \rho_g C_{pg}}{K_g}} \quad . \tag{2.4}$$

The density of the gas inside the bubble is $\rho_g$, $C_{pg}$ is the specific heat of the gas at constant pressure, and $K_g$ is the thermal conductivity of the gas.

The resonance frequency $f_r$ is given by[6]

$$f_r = \frac{\sqrt{\frac{3\gamma b \beta P_0}{\rho}}}{2\pi r_b} \quad , \tag{2.5}$$

4

where $P_0$ is the ambient static pressure and $\rho$ is the density of the surrounding medium; b and $\beta$ are quantities which must be included to account for the surface tension $\tau$ of the bubble wall and the thermal conductivity $K_g$ of the gas inside the bubble:

$$b = \left[1+\left(\frac{d}{b}\right)^2\right]^{-1}\left[1+\frac{3(\gamma-1)}{X}\left(\frac{\sinh X-\sin X}{\cosh X-\cos X}\right)\right]^{-1} \tag{2.6}$$

$$\beta = 1 + \frac{2\tau}{P_0 r_b}\left(1-\frac{1}{3\gamma b}\right) \quad . \tag{2.7}$$

The ambient density $\rho$ appears in Eqs. (2.2) and (2.5). In the simple case of a pure fluid medium, $\rho$ is simply the density of the fluid. When the medium surrounding the bubble contains sediment particles, the effective fluid density presented in Sec. 2.3 must be used.

## 2.2 RELATIONSHIP BETWEEN INCIDENT AND BACKSCATTERED PRESSURE

In this section, a general expression for the backscattered pressure from an element of sediment volume is derived. In Sec. 2.2.1 the relationship between pore fluid acoustic pressure and velocity is presented. In Sec. 2.2.2, an expression for the pore fluid acoustic impedance is developed. In Sec. 2.2.3 the principle of acoustic reciprocity is used to develop an expression for the backscattered pressure from a sediment volume element. This backscattered pressure is expressed in terms of the pressure incident upon the scattering element, which can be obtained with the Biot model, described in Sec. 2.3.

### 2.2.1 Relationship between Acoustic Pressures and Fluid Velocities

The linear wave equation in a fluid medium is given by

$$\nabla^2 p = \frac{1}{c^2}\frac{\partial^2 p}{\partial t^2} \quad , \tag{2.8}$$

5

where c is the phase velocity of a compressional wave in the fluid. For a pressure field that is spherically symmetric about a source at the origin, there is only radial dependence. The $\nabla^2$ operator in this case is given by

$$\nabla^2 = \frac{\partial^2}{\partial r^2} + \frac{2}{r}\frac{\partial}{\partial r} \quad . \tag{2.9}$$

Upon substitution of Eq. (2.9) into Eq. (2.8) and rearrangement, the wave equation can be written in the form

$$\frac{\partial^2(rp)}{\partial r^2} = \frac{1}{c^2}\frac{\partial^2(rp)}{\partial t^2} \quad . \tag{2.10}$$

General solutions for the quantity rp can be expressed as

$$rp = f_1(ct-r) + f_2(ct+r) \quad , \tag{2.11}$$

where the first term represents a general incoming wave and the second term a general outgoing wave. If we consider outgoing harmonic waves only, the pressure field can be expressed as

$$p = \frac{A}{r}\exp(i(kr-\omega t)) \quad , \tag{2.12}$$

where **A** is an arbitrary complex amplitude, $k=\omega/c+i\alpha$ is the acoustic wavenumber, $\alpha$ is the absorption in Np/m, and $\omega=2\pi f$ is the angular frequency. For small amplitude signals the fluid velocity is related to the acoustic pressure according to Euler's equation,[7]

$$\rho_0\frac{\partial \vec{v}}{\partial t} = -\nabla p \quad , \tag{2.13}$$

where $\rho_0$ is the average density of the medium. Upon combination of Eqs. (2.12) and (2.13), a relation between acoustic pressure and fluid velocity is obtained,

$$\vec{v} = \hat{r}\left(1 - \frac{i}{kr}\right)\frac{p}{\rho_0 c} \quad , \tag{2.14}$$

where $\hat{r}$ is the unit vector in the radial direction.

## 2.2.2 Acoustic Impedance

The acoustic impedance is defined in terms of the acoustic pressure and fluid velocity,

$$Z_I = \frac{d\,p_I}{d\,v_I} \quad , \tag{2.15}$$

where $v_I$ is the velocity component in the direction of the velocity vector $\vec{v}$. For small amplitude signals Eq. (2.15) simplifies to

$$Z_I = \frac{p_I}{v_I} \quad . \tag{2.16}$$

Equations (2.14) and (2.16) can be combined to form an expression for the acoustic impedance:

$$Z_I = \frac{\rho_i c}{\left(1 - \frac{i}{k_I r}\right)} \quad . \tag{2.17}$$

At large distances from the source, where $k_I r$ is large, the impedance of Eq. (2.17) reduces to the plane wave acoustic impedance $Z_i = \rho_i c$.

## 2.2.3 Backscattered Pressure from an Element dxdydz of Sediment Volume by Reciprocity

Consider the situation where the scatterer is an element of sediment volume dxdydz. In this case it is convenient to surround the source and scatterer with virtual spheres with radius r much greater than the acoustic wavelength $\lambda$, as illustrated in Fig. 2.1.
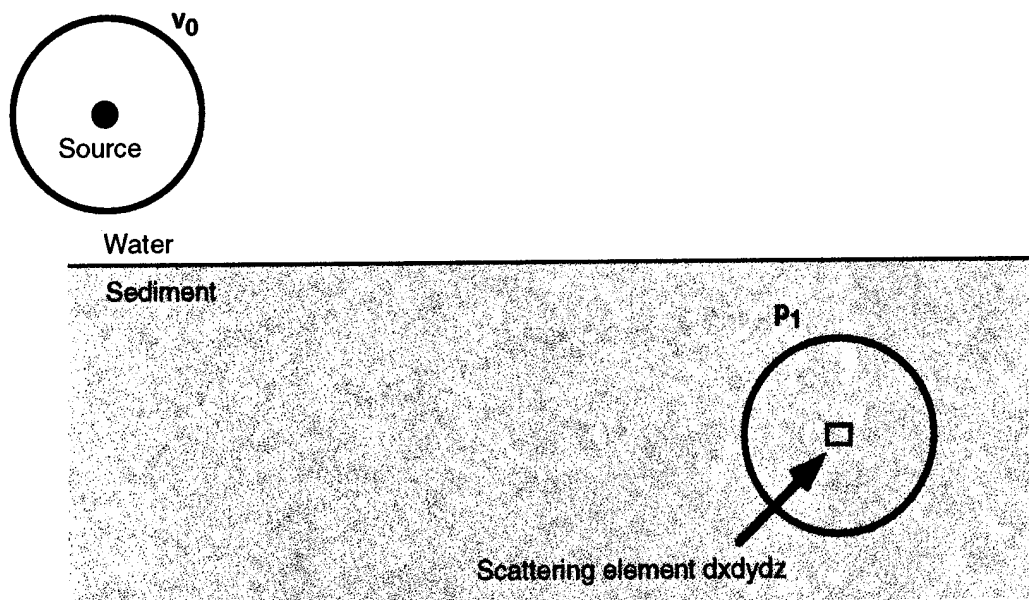
(a) Acoustic propagation of incident sound.
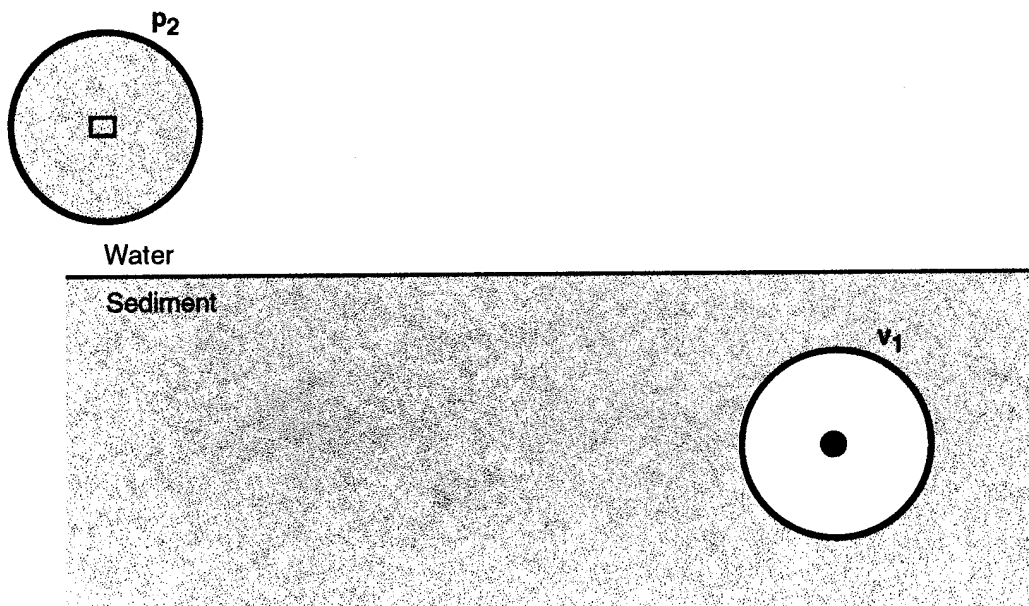


(b) Acoustic propagation of backscattered sound.

**Figure 2.1**
**Calculation of backscattered pressure by reciprocity.**

Reciprocity is applied to virtual spheres of equal radius about source and scatterer. The radius is much greater than the acoustic wavelength so that plane wave acoustic impedances can be used, and much smaller than the separation between source and scatterer so that the projected pressures $|p_1|$ and $|p_2|$ are approximately constant across the spheres' surfaces.

8

The spherical surface surrounding the source has a surface velocity $v_0$, which generates a pressure $p_1$ at the location of the scatterer. The scatterer responds with a scattered surface velocity $v_1$, which induces a backscattered pressure $p_2$ at the source. These pressures and surface velocities can be related by acoustic reciprocity, which states that, in a linear medium, a source and receiver can be swapped with no change in the ratio of received to transmitted signals. This swapping of positions can be interpreted to represent the backscatter case, where the scatterer acts as a projector and the source as a receiver. In terms of pressures and velocities, the reciprocity principle states:

$$\frac{p_1}{v_0} = \frac{p_2}{v_1} \quad . \tag{2.18}$$

By inversion of Eq. (2.16), the fluid velocities at the virtual surfaces of the projector and scatterer can be expressed in terms of local pressures and impedances:

$$v_0 = \frac{p_0}{Z_0} \tag{2.19}$$

and

$$v_1 = \frac{\varepsilon p_1}{Z_1} \quad , \tag{2.20}$$

where $v_0$, $p_0$, and $Z_0$ are the fluid velocity, the acoustic pressure, and the impedance at the surface of the virtual sphere surrounding the projector. $v_1$ and $Z_1$ are the scattered fluid velocity and the acoustic impedance at the virtual sphere surrounding the scatterer. $\varepsilon$ is a transfer function, from incident pressure $p_1$ to scattered pressure $\varepsilon p_1$ at the surface of the scatterer's virtual sphere. It includes the effects of sound pressure generation by the scattering element $dxdydz$ as an effective source, as well as propagation of this pressure to the virtual sphere surface. As illustrated in Fig. 2.1, this propagation must take place as if it were in the water column. If we neglect the attenuation in the water column, the average square magnitude of $\varepsilon$ is

$$\langle |\varepsilon|^2 \rangle = \frac{\sigma_{bv} \, dxdydz}{4\pi r_s^2} \quad , \tag{2.21}$$

where dxdydz is the sediment volume element and $r_s$ is the radius of the virtual spheres surrounding source and scatterer. $\sigma_{bv}$ is the volume scattering cross section, defined as ratio of scattered power to incident intensity for the sediment volume scattering element, averaged over the complete ensemble of possible bubble distributions within dxdydz. By combination of Eqs. (2.18), (2.19), (2.20), and (2.21), an expression for the square magnitude of the acoustic pressure returned to the projector from the scattering element dxdydz is obtained:

$$\langle |p_2|^2 \rangle = \int \left| \frac{p_1}{p_0} \right|^2 \frac{\sigma_{bv}}{4\pi r_s^2} \left| \frac{Z_0}{Z_1} p_1 \right|^2 dxdydz \quad . \tag{2.22}$$

This quantity is proportional to the power returned to the projector from the scattering element.

Since the radius of the virtual spheres was assumed large in comparison to the wavelength $\lambda$, plane wave acoustic impedances can be used for $Z_0$ and $Z_1$:

$$|Z_0| = \left| \frac{p_0}{v_0} \right| = \rho_0 c_0 \tag{2.23}$$

and

$$|Z_1| = \left| \frac{p_1}{v_1} \right| = \rho_1 c_1 \quad , \tag{2.24}$$

where $p_0$, $v_0$, $p_1$, and $v_1$ are plane wave acoustic pressures and fluid velocities in the water column and sediment, respectively. $\rho_0$ and $\rho_1$ are densities of the water and sediment and $c_0$ and $c_1$ are corresponding phase velocities.

## 2.3 CALCULATION OF PORE PRESSURES AND EFFECTIVE DENSITIES WITH THE BIOT THEORY

For a sandy sediment, $p_1$ and $v_1$ can be obtained via the Biot model, described in Ref. 2. The Biot model predicts fast and slow compressional waves in the pore fluid. Since shear waves do not couple strongly into the pore fluid, they can be neglected. Each wave will have its own fluid velocity and pressure. The pore fluid is therefore assigned two partial acoustic impedances,[8] one for each of the Biot compressional waves.

$$Z_{1f} = \frac{p_{1f}}{v_{1f}} \tag{2.25}$$

and

$$Z_{1s} = \frac{p_{1s}}{v_{1s}} \quad , \tag{2.26}$$

where the subscript 1 corresponds to the pore fluid and the subscripts f and s correspond to the fast and slow waves, respectively.

The pore fluid also has two effective densities, one for each of the Biot waves that the medium supports:

$$\rho_{fast} = \frac{|Z_{1f}|}{c_f} \tag{2.27}$$

and

$$\rho_{slow} = \frac{|Z_{1s}|}{c_s} \quad , \tag{2.28}$$

where $c_f$ and $c_s$ are the fast and slow wavespeeds, obtainable via the Biot model.

The simultaneous presence of the fast and slow acoustic waves affects the form of the returned pressure from a scattering element, Eq. (2.22). For scattering within a Biot medium, the expression for the magnitude squared backscattered pressure is

$$\left\langle |p_2|^2 \right\rangle = \int \left| \frac{p_1}{p_0} \right|^2 \left( \frac{\sigma_{bvf}}{4\pi r_s^2} \left| \frac{Z_0}{Z_{1f}} p_{1f} \right|^2 + \frac{\sigma_{bvs}}{4\pi r_s^2} \left| \frac{Z_0}{Z_{1s}} p_{1s} \right|^2 \right) dxdydz \quad , \tag{2.29}$$

where $p_1$ in this expression is the total pore pressure, $p_{1f} + p_{1s}$, due to fast and slow waves.

$\sigma_{bvf}$ and $\sigma_{bvs}$ are the ensemble average volume scattering cross section densities for fast and slow waves, respectively. They represent the collective backscatter contributions from all the trapped bubbles in the sediment and have sensitive dependence on the size distribution of trapped bubbles. The

11

distribution of bubble radii is assumed proportional to the distribution of pore radii, with the proportionality factor $r_{bp}$:

$$r_{bp} = \text{bubble radius/pore radius} \quad . \tag{2.30}$$

The distribution of pore radii is related to the distribution of grain radii, which can be measured. This relationship is detailed in Ref. 2.

An expression for the bubble size distribution, on which these scattering cross sections are based, is detailed in Ref. 2 and is based on a bubble size distribution that mirrors the sediment pore size distribution. Given a pore size distribution, which can be estimated from the grain size distribution, the bubble size distribution is specified by a single parameter, $r_{bp}$, that specifies the bubble size to pore size ratio.

## 2.4    SEDIMENT INTERFACE BACKSCATTERING STRENGTH

In this section, the backscatter contribution from a sediment volume element, given by Eq. (2.29), is used to determine the backscattering strength of the sediment interface. In order to specify an interface backscattering strength, scattering from within the sediment volume must be recast as "effective" interface scattering. As illustrated in Fig. 2.2, one can define the backscattered intensity from an interface element, dxdy, as the sum of backscattered intensities from all volume elements dxdydz below dxdy.

This definition of the interface backscattering contribution is based on the assumption of plane waves incident upon the interface. The resulting backscatter model will therefore be most applicable when the sediment interface is far from the projector, i.e., when wavefront curvature is negligible in comparison with acoustic penetration depth into the sediment.

The average magnitude squared of the backscattered pressure $|p_{bs}|^2$ returned to the projector from the sediment, per unit area of interface, is given by

Projector;
backscattered p = pbs

●

Surface element dxdy

Incident ray

Volume scattering
elements dxdydz
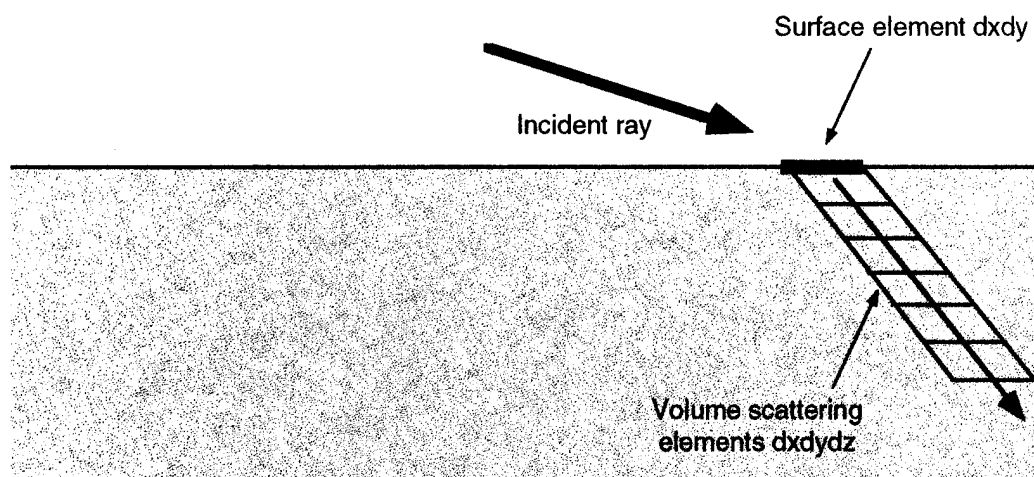
**Figure 2.2**
**Backscatter from the volume below surface element dxdy.**

$$\langle |p_{bs}|^2 \rangle = \int_0^\infty \left|\frac{p_1}{p_0}\right|^2 \left( \frac{\sigma_{bvf}}{4\pi r_s^2} \left|\frac{Z_0}{Z_{1f}} p_{1f}\right|^2 + \frac{\sigma_{bvs}}{4\pi r_s^2} \left|\frac{Z_0}{Z_{1s}} p_{1s}\right|^2 \right) dz \qquad . \qquad (2.31)$$

The backscattering strength of an interface element is defined as

$$BS = 10 \log \frac{\langle |p_s|^2 \rangle}{|p_{inc}|^2} \qquad , \qquad\qquad (2.32)$$

where $p_s$ is the backscattered pressure at unit distance $r_{1m}$ from the interface element and $p_{inc}$ is the pressure incident upon interface, as illustrated in Fig. 2.3. These pressures are related to $p_{bs}$ and $p_0$ in the following way:

$$|p_s| = |p_{bs}| \frac{r}{r_{1m}} e^{r\alpha} \qquad , \qquad\qquad (2.33)$$

$$|p_{inc}| = |p_0| \frac{r_s}{r} e^{-r\alpha} \qquad , \qquad\qquad (2.34)$$

where $r$ is the separation between the projector and the interface element and $\alpha$ is the absorption coefficient of the water column in units of nepers per unit distance. By combining Eqs. (2.31), (2.32), (2.33), and (2.34), the backscattering strength of an interface element of unit area is expressible in terms of $p_0$ and $p_1$:

$$BS = 10 \log \left( \frac{\left(\dfrac{r^4}{r_{1m}^2 r_s^4}\right) \displaystyle\int_0^\infty |p_1|^2 \left( \dfrac{\sigma_{bvf}}{4\pi} \left|\dfrac{Z_0}{Z_{1f}} p_{1f}\right|^2 + \dfrac{\sigma_{bvs}}{4\pi} \left|\dfrac{Z_0}{Z_{1s}} p_{1s}\right|^2 \right)}{|p_0|^4} \right)$$
$$+ 40 \log(e) \, r\alpha \qquad . \qquad\qquad (2.35)$$

In terms of the incident pressure $p_{inc}$ at the interface, the backscattering strength is

**Figure 2.3**
**Incident and scattered pressures**
**as defined for an interface scattering element.**

$$BS = 10 \log \left( \frac{\left( \frac{1}{r_{1m}^2} \right) \int_0^\infty |p_1|^2 \left( \frac{\sigma_{bvf}}{4\pi} \left| \frac{Z_0}{Z_{1f}} p_{1f} \right|^2 + \frac{\sigma_{bvs}}{4\pi} \left| \frac{Z_0}{Z_{1s}} p_{1s} \right|^2 \right)}{|p_{inc}|^4} \right) \quad , \quad (2.36)$$
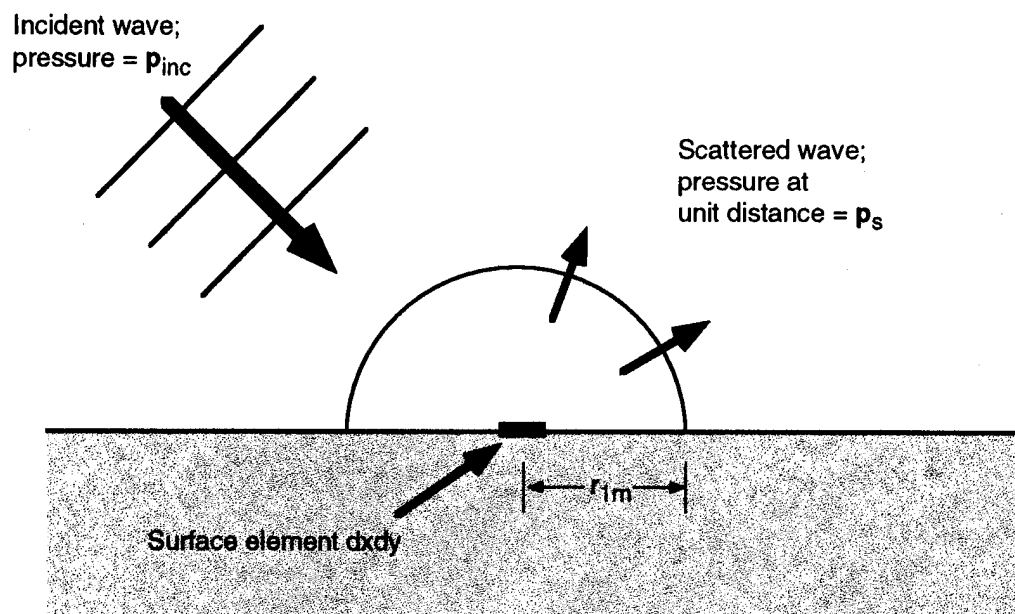
where $p_{inc}$ is given by Eq. (2.34).

# 3. COMPARISON OF THEORY WITH EXPERIMENT

Figure 3.1 is a comparison of model predictions with backscatter measurements from four selected sites.[9-12] Backscattering strengths are plotted against normalized grain size, which is proportional to frequency as follows:

$$\text{normalized grain size} = \frac{\text{frequency * mean grain diameter}}{\text{sound speed in water}} . \qquad (3.1)$$

The input parameters for each site are listed in Table 3.1. In each case a best fit was obtained by varying the gas fraction $\zeta$ and the bubble to pore radius ratio ($r_{bp}$). The resulting gas fractions varied between $1 \times 10^{-6}$ and $1 \times 10^{-5}$, and $r_{bp}$s varied between 1.71 and 8.43.

The fact that the bubble to pore radius ratios $r_{bp}$ were greater than unity appears to have the unphysical implication that trapped bubbles are larger than their surrounding pores. One possible explanation for this is that the assumption that bubble size distributions mirror the pore size distributions may be inaccurate. Surface tension, for example, may force very small bubbles into solution, skewing the distribution toward bubbles of larger radii. Such an effect would affect bubble distributions in fine grained sands more severely than those in coarse grained sands. The idea that the bubble size distribution may favor larger radii than the pore size distribution is supported by the fact that, as shown in Table 3.1, $r_{bp}$ increases steadily with decreasing mean grain size. Other possible explanations for the large $r_{bp}$s are that bubbles in neighboring pores coalesce or couple acoustically, or that other mechanisms besides trapped bubbles contribute to the backscattering strengths.

By varying the two free parameters, the behavior of the model can be adjusted to match observations well. The observed peak in backscattering strength is matched by the model, given appropriate values for $\zeta$ and $r_{bp}$. As a result, very small gas fractions are inferred. At present the authors are aware of no practical way of measuring such small gas fractions in sediments.

**Kings Bay, 1985**

Gas fraction ................................ $1\times10^{-6}$

Bubble:pore radius ratio ($r_{bp}$)..... 3.11



Backscattering strength - dB

Normalized grain size

**Jacksonville, 1989**

Gas Fraction $2\times10^{-6}$

$r_{bp}$................1.71



Backscattering strength - dB

Normalized grain size

**Panama City, 1986**

Gas Fraction $1\times10^{-5}$

$r_{bp}$................8.43



Backscattering strength - dB

Normalized grain size

**McKinney and Anderson, 1964**

Gas Fraction $1\times10^{-5}$

$r_{bp}$............. 8.43



Backscattering strength - dB

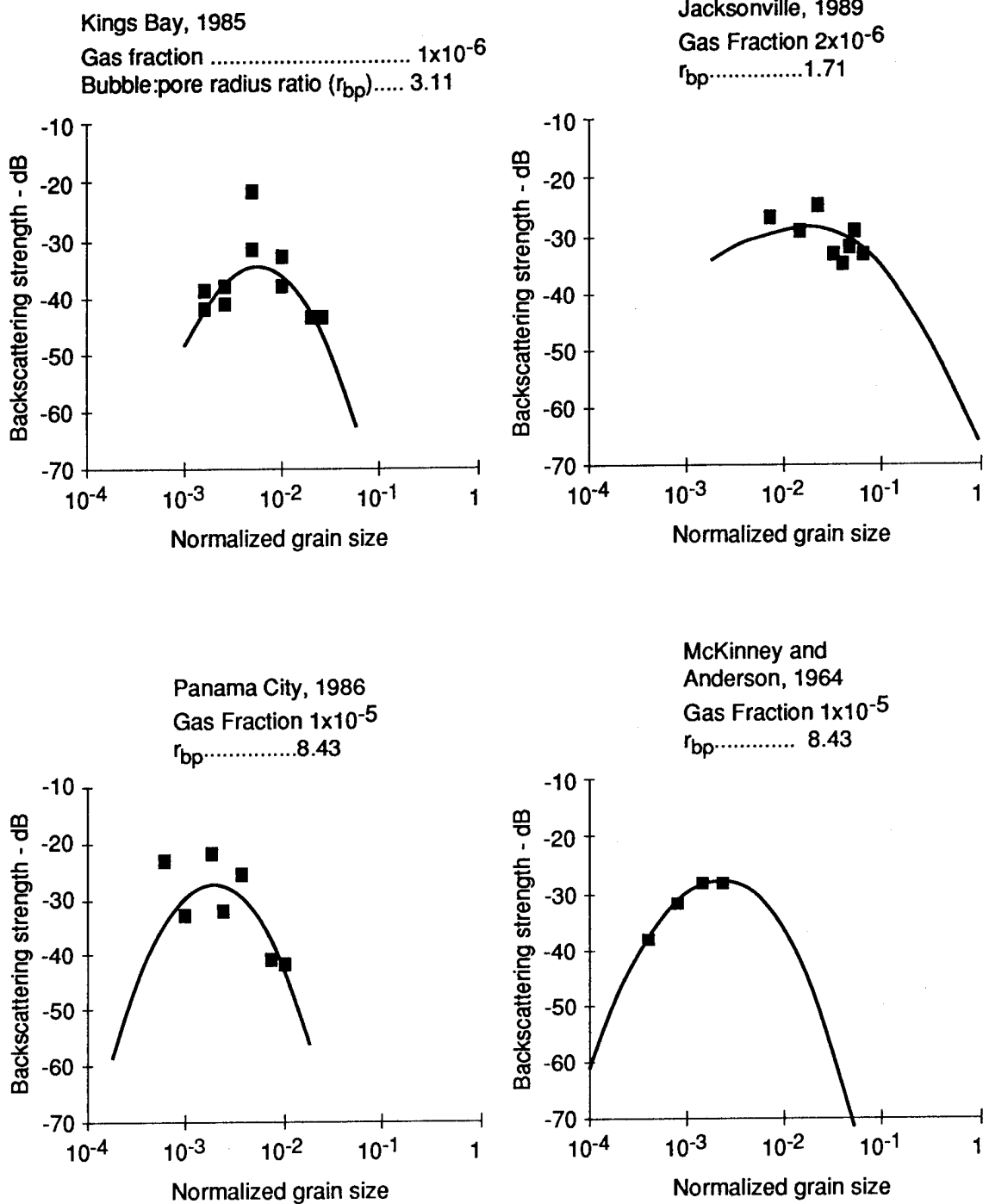Normalized grain size

**Figure 3.1**
**Comparison of experimental data with**
**backscattering strengths predicted by Eq. (2.36).**

## Table 3.1
## Backscatter model site parameters.

| Parameter | Unit of Measure | Kings Bay 1985 | Panama City 1986 | Jacksonville 1989 | McKinney et al. 1964 |
|---|---|---|---|---|---|
| Fluid density | $(kg/m^3)$ | 1000 | 1000 | 1000 | 1000 |
| Fluid bulk modulus | (Pa) | $2.25 \times 10^9$ | $2.25 \times 10^9$ | $2.25 \times 10^9$ | $2.25 \times 10^9$ |
| Porosity | | 0.36 | 0.39 | 0.38 | 0.4 |
| Grain density | $(kg/m^3)$ | 2650 | 2650 | 2650 | 2650 |
| Mean grain diameter | $(\phi)$ | 1.30 | 2.51 | 0.84 | 3.0 |
| Standard deviation | $(\phi)$ | 0.86 | 0.79 | 1.6 | 1.0 |
| Pore size parameter | (m) | $1.09 \times 10^{-4}$ | $5.08 \times 10^{-5}$ | $3.89 \times 10^{-4}$ | $4.49 \times 10^{-5}$ |
| Viscosity | (kg/m-s) | $1.0 \times 10^{-3}$ | $1.0 \times 10^{-3}$ | $1.0 \times 10^{-3}$ | $1.0 \times 10^{-3}$ |
| Permeability | $(m^2)$ | $2.15 \times 10^{-10}$ | $5.03 \times 10^{-11}$ | $2.87 \times 10^{-9}$ | $4.03 \times 10^{-11}$ |
| Virtual mass parameter | | 1.889 | 1.782 | 1.818 | 1.75 |
| Grain bulk modulus | (Pa) | $7.0 \times 10^9$ | $7.0 \times 10^9$ | $7.0 \times 10^9$ | $7.0 \times 10^9$ |
| Frame shear modulus | (Pa) | $2.61 \times 10^7$ | $2.61 \times 10^7$ | $2.61 \times 10^7$ | $2.61 \times 10^7$ |
| Shear log decrement | | 0.15 | 0.15 | 0.15 | 0.15 |
| Frame bulk modulus | (Pa) | $5.3 \times 10^9$ | $5.3 \times 10^9$ | $5.3 \times 10^9$ | $5.3 \times 10^9$ |
| Bulk log decrement | | 0.15 | 0.15 | 0.15 | 0.15 |
| Gas bulk modulus | (Pa) | $2.48 \times 10^5$ | $2.48 \times 10^5$ | $2.48 \times 10^5$ | $2.48 \times 10^5$ |
| Gas density | $(kg/m^3)$ | 1.22 | 1.22 | 1.22 | 1.22 |
| Gas heat conductivity | (cal/m-s-$^{o}$c) | $5.6 \times 10^{-3}$ | $5.6 \times 10^{-3}$ | $5.6 \times 10^{-3}$ | $5.6 \times 10^{-3}$ |
| Gas specific heat (const press) | (cal/kg) | 240 | 240 | 240 | 240 |
| Gas specific heat ratio, $C_p/C_v$ | | 1.4 | 1.4 | 1.4 | 1.4 |
| Bubble surface tension | $(N/m^2)$ | 0.075 | 0.075 | 0.075 | 0.075 |
| Bubble:pore radius ratio | | 3.11 | 8.43 | 1.71 | 8.43 |
| Gas content | | $1.0 \times 10^{-6}$ | $1.0 \times 10^{-5}$ | $2.0 \times 10^{-6}$ | $1.0 \times 10^{-5}$ |

This page intentionally left blank.

# 4. SUMMARY AND CONCLUSIONS

A model has been developed to predict acoustic backscatter from gas bubbles trapped in the pores of a sandy sediment. The model incorporates a Biot acoustic propagation model and allows for scattering of both fast and slow waves. The effects of bubble confinement within sediment pores on bubble resonances and acoustic scattering cross sections are included.

The new model has two free input parameters, the gas fraction and the bubble to pore radius ratio. Since there is currently no method of measuring either of them, they are simply adjusted to fit the model to measured data. By adjusting these parameters, it is possible to get the model to fit data collected experimentally at several sites. The fit includes a broad peak that sometimes occurs in the backscattering strength spectrum that cannot be explained with other models.

A very small gas fraction of between $10^{-5}$ and $10^{-6}$ was sufficient to get the model to match the observed backscatter. These gas fractions are smaller than can be measured at present so there is no independent verification of the model.

There are reasons to expect gas in shallow water sediments.[13] Gas bubbles have been observed in core samples of marine sediments, as well as in echo soundings, which have recorded bubbles escaping to the surface. This suggests that trapped bubbles may be significant in high frequency acoustic backscatter from sediments.

The large values of the bubble to pore radius ratio suggest that the assumed shape of the bubble size distribution function is inaccurate. The fact that $r_{bp}$ increases steadily with decreasing mean grain size suggests that the actual bubble size distribution contains fewer small bubbles and more large bubbles. A study of other factors, besides pore size, that might affect bubble size may allow a better estimate of the bubble size distribution.

This page intentionally left blank.

# REFERENCES

1.  F. A. Boyle and N. P. Chotiros, "Bottom Penetration at Shallow Grazing Angles II," Applied Research Laboratories Technical Report No. 92-12 (ARL-TR-92-12), Applied Research Laboratories, The University of Texas at Austin, June 1992.

2.  F. A. Boyle and N. P. Chotiros, "Bottom Backscatter from Trapped Bubbles," Applied Research Laboratories Technical Report No. 93-15 (ARL-TR-93-15), Applied Research Laboratories, The University of Texas at Austin, July 1993.

3.  L. E. Kinsler, A. R. Frey, A. P. Coppens, and J. V. Sanders, *Fundamentals of Acoustics* (Wiley, New York, 1982).

4.  R. J. Urick, *Principles of Underwater Sound* (Mcgraw-Hill, New York, 1975).

5.  R. Wildt, ed., "Acoustic Theory of Bubbles," *Physics of Sound in the Sea*, N.D.R.C. Summary Technical Report, Div. 6, Chap. 28, Vol. 8, Washington, DC (1946).

6.  H. Medwin, "Counting Bubbles Acoustically, A Review," Ultrasonics 7-13 (1977).

7.  Kinsler, Frey, Coppens, and Sanders, *Fundamentals of Acoustics*.

8.  J. I. Dunlop, "Propagation of acoustic waves in marine sediments, a review," Exploration Geophysics **19**, 513-535 (1988).

9.  N. P. Chotiros and H. Boehme, "Analysis of Bottom Backscatter Data from the Kings Bay Experiment," Applied Research Laboratories Technical Report No. 88-6 (ARL-TR-88-6), Applied Research Laboratories, The University of Texas at Austin, January 1988.

10. S. Stanic, K. B. Briggs, P. Fleischer, W. B. Sawyer, and R. I. Ray, "High-frequency acoustic backscattering from a coarse shell ocean bottom," J. Acoust. Soc. Am. **85**(1), 125-136 (1989).

11. N. P. Chotiros, "High Frequency Bottom Backscattering: Panama City Experiment," Applied Research Laboratories Technical Report No. 90-22 (ARL-TR-90-22), Applied Research Laboratories, The University of Texas at Austin, July 1990.

12. C. M. McKinney and C. D. Anderson, "Measurements of backscattering of sound from the ocean bottom," J. Acoust. Soc. Am **36**, 158-163 (1964).

13. A. L. Anderson and L. D. Hampton, "Acoustics of gas-bearing sediments," J. Acoust. Soc. Am. **67**(6) 1865-1903 (1980).

# DISTRIBUTION LIST FOR
## ARL-TR-94-21
### Final Report under Contract N00039-91-C-0082,
### TD No. 01A2063
### Bottom Backscatter From Trapped Bubbles - II

<u>Copy No.</u>

Commanding Officer
Naval Research Laboratory
Stennis Space Center, MS  39529-5004

| | |
|---|---|
| 1 | Attn:  S. Stanic (Code 7174) |
| 2 | D. Ramsdale (Code 7170) |
| 3 | D. Young (Code 7331) |
| 4 | P. Fleischer (Code 7431) |
| 5 | K. Briggs (Code 7431) |
| 6 | P. Valent (Code 7400) |
| 7 | R. Love (Code 7174) |
| 8 | E. Franchi (Code 7100) |
| 9 | M. Richardson (Code 7431) |
| 10 | R. Meredith (Code 7474) |
| 11 - 22 | Library (Code 7032.2) |

Office of Naval Research
Department of the Navy
Arlington, VA  22217-5000

| | |
|---|---|
| 23 | Attn:  J. Kravitz (Code 322) |
| 24 | J. Simmen (Code 321) |
| 25 | E. Chaika (322) |
| 26 | W. Ching (Code 321) |
| 27 | T. Goldsberry (Code 322) |
| 28 | D. Houser (Code 333) |

Commanding Officer
Naval Oceanographic Office
Stennis Space Center, MS  32529

| | |
|---|---|
| 29 | Attn:  J. Bunce (Code N31) |
| 30 | E. Beeson (Code N3) |

Commanding Officer
Naval Meteorology & Oceanography Command
Stennis Space Center, MS  32529

| | |
|---|---|
| 31 | Attn:  D. Durham (Code N5A) |
| 32 | R. L. Martin (Code N5C) |

Distribution List for ARL-TR-94-21 under Contract N00039-91-C-0082,
TD No. 01A2063
(cont'd)

<u>Copy No.</u>

Commander
Naval Sea Systems Command
Department of the Navy
Washington, DC  20362-5101
33          Attn:     J. Grembi (PMO407)
34                    D. Gaarde (PMO407)

G & C Systems Manager
MK48/ADCAP Program Office
National Center 2
2521 Jefferson Davis Hwy
12W32
Arlington, VA  22202
35          Attn:     H. Grunin (PMO402E1)

Program Manager
MK50 Torpedo Program Office
Crystal Park 1
2011 Crystal Drive
Suite 1102
Arlington, VA  22202
36          Attn:     A. Knobler (PMO406B)

Commander
Dahlgren Division
Naval Surface Warfare Center
Dahlgren, VA  22448-5001
37          Attn:     Library

Commander
Dahlgren Division
Naval Surface Warfare Center
Silver Spring, MD  20903-5000
38          Attn:     S. Martin (Code G94)
39                    J. Sherman (Code N50)
40                    M. Stripling (Code N04W)

Distribution List for ARL-TR-94-21 under Contract N00039-91-C-0082,
TD No. 01A2063
(cont'd)

<u>Copy No.</u>

|     | Commanding Officer<br>Coastal Systems Station, Dahlgren Division<br>Naval Surface Warfare Center<br>Panama City, FL  32407-7001 |
| --- | --- |
| 41  | Attn:    M. Hauser (Code 10CD) |
| 42  | R. Lim (Code 130B) |
| 43  | E. Linsenmeyer (Code 10P) |
| 44  | D. Todoroff (Code 130) |

|     | Commander<br>Naval Undersea Warfare Center Division<br>New London, CT  06320-5594 |
| --- | --- |
| 45  | Attn:    J. Chester (Code 3112) |
| 46  | P. Koenig (Code 33A) |

|     | Advanced Research Projects Agency<br>3701 North Fairfax Drive<br>Arlington, VA  22203-1714 |
| --- | --- |
| 47  | Attn:    W. Carey |

|     | Commander<br>Naval Undersea Warfare Center Division<br>Newport, RI  02841-5047 |
| --- | --- |
| 48  | Attn:    J. Kelly (Code 821) |
| 49  | F. Aidala (Code 842) |
| 50  | W. Gozdz (Code 843) |

|     | Officer in Charge<br>Arctic Submarine Lab Detachment<br>Naval Undersea Warfare Center<br>49250 Fleming Rd.<br>San Diego, CA  92152-7210 |
| --- | --- |
| 51  | Attn:    R. Anderson (Code 19) |

|     | Chief of Naval Operations<br>Department of the Navy<br>Washington, DC  20350-2000 |
| --- | --- |
| 52  | Attn:    R. Widmayer (N852T) |
| 53  | H. Montgomery (N911) |
| 54  | J. Boosman (N911D2) |

Distribution List for ARL-TR-94-21 under Contract N00039-91-C-0082,
TD No. 01A2063
(cont'd)

Copy No.

Commander
Mine Warfare Command
325 5th Street SE
Corpus Christi, TX 78419
55          Attn:      G. Pollitt (Code N02R)

Commanding Officer and Director
Defense Technical Information Center
Cameron Station, Building 5
5010 Duke Street
56 - 67     Alexandria, VA 22314

Applied Physics Laboratory
The University of Washington
1013 NE 40th Street
Seattle, WA 98105
68          Attn:      D. Jackson
69                     S. Kargl
70                     Library

Applied Research Laboratory
The Pennsylvania State University
P. O. Box 30
State College, PA 16804-0030
71          Attn:      R. Goodman
72                     E. Liszka
73                     D. McCammon
74                     F. Symons
75                     Library

Presearch, Inc.
8500 Executive Park Avenue
Fairfax, VA 22031
76 - 79     Attn:      J. R. Blouin

Ocean Engineering Department
Massachusetts Institute of Technology
77 Massachusetts Avenue
Cambridge, MA 02139
80          Attn: R. J. Fricke

Physics Department
The University of Texas at Austin
Austin, TX 78712

| | |
|---|---|
| 81 | Attn: W. D. McCormick |
| 82 | M. Fink |
| 83 | T. Griffy |

Aerospace Engineering Department
The University of Texas at Austin
Austin, TX 78712

| | |
|---|---|
| 84 | Attn: M. Stern |
| 85 | Robert A. Altenburg, ARL:UT |
| 86 | Hollis Boehme, ARL:UT |
| 87 | Frank A. Boyle, ARL:UT |
| 88 | Nicholas P. Chotiros, ARL:UT |
| 89 | John M. Huckabay, ARL:UT |
| 90 | Thomas G. Muir, ARL:UT |
| 91 - 97 | Reserve, Advanced Sonar Group, ARL:UT |
| 98 | Library, ARL:UT |